Sixth International Symposium on Turbulence and Shear Flow Phenomena
Seoul, Korea, 22-24 June 2009

MODIFICATION OF FLOW AROUND A CIRCULAR CYLINDER USING POROUS MEDIA

Hiroshi Naito, Koji Fukagata, and Shinnosuke Obi
Department of Mechanical Engineering, Keio University
3-14-1 Hiyoshi; Kohoku-ku, Yokohama, 223-8522, Japan,
piroshi21@a8.keio.jp

ABSTRACT

Flow around a circular cylinder having a porous surface is studied numerically by means of direct numerical simulation (DNS) and large eddy simulation (LES). The flow in the porous media is represented by a spatially-averaged (i.e., macroscopic) model. The parameters of the most effective porous media are found from a two-dimensional parametric test at the Reynolds number, based on the free stream velocity and the diameter of cylinder, of $Re = 1000$. The lift force fluctuation is notably reduced in the case of thicker porous surface. The DNS of three-dimensional flow at $Re = 1000$ reveals that the porous surface works to stabilize the shear layer. The LES at a very high Reynolds number ($Re = 10^5$) shows that the vortex shedding is completely suppressed by the porous media, which supports the experimental observation by Sueki et al. (2007). Simulations at different Reynolds numbers show that the stabilization effect works better at higher Reynolds numbers.

INTRODUCTION

Vortex shedding from a circular cylinder causes many engineering problems, such as noise, large drag and oscillation due to the lift force, which in the worst case yield breakage of instruments. In order to resolve these problems, flow control around a circular cylinder has been studied by many researchers (Choi et al., 2008).

Recently, Sueki et al. (2007) investigated the effect of porous media fitted around a cylinder aiming at noise reduction of pantograph and achieved considerable reduction of noise. Its mechanism was explored by the same group using the PIV measurement (Takaishi et al., 2007): they observed apparent modification of the downstream wake. These results suggest that the porous media is an effective control device for flow around a bluff body.

Toward the use of porous media in industral applications, one should further accumulate the knowledge about its effect on the flow, including the dependency to various design parameters and the detailed mechanism of flow modification. Therefore, in the present study, we perform simulation of flow around a circular cylinder having a porous surface by means of direct numerical simulation (DNS) and large eddy simulation (LES). First, we perform a parametric test for two-dimensional (2D) flow at the Reynolds number, based on the free stream velocity and the diameter of cylinder, of $Re = 1000$, and the flow fields in some selected cases are analyzed in detail. Subsequently, three-dimensional (3D) simulation is performed at $Re = 1000$ in order to investigate the 3D effect. Moreover, the simulation is performed for a lower Reynolds number ($Re = 100$) and a higher Reynolds number ($Re = 10^5$) in order to clarify the Reynolds number dependency.

NUMERICAL DETAILS

We consider the flow around a circular cylinder having a porous surface. Various simulation methods have been proposed to treat the flow faced on porous surface:

1. direct method, in which the complex geometry of porous media is treated directly (Martys and Chen, 1996);

2. method of boundary condition, which uses an artificial boundary condition mimicking the effect of porous surface (Jiménez et al., 2001);

3. macroscopic flow model, which uses a volume-averaged equation in the porous media (Bruneau and Mortazavi, 2004).

In this study, we adopt the last method to avoid numerical complexity and to study the effect of porous media thickness.

The momentum equation for an isothermal, incompressible flow including that in the porous media is given by (Hsu and Cheng, 1990):

$$\frac{\partial u}{\partial t} + \left(\overline{u \cdot u}\right) = \quad p + \frac{1}{Re} \quad ^2u + K \ , \qquad (1)$$

where

$$K = \quad \overline{ReDa}u \quad \frac{1.75}{\sqrt{150}} \frac{1}{\sqrt{Da}} \frac{u|u|}{\sqrt{\ }} \ . \qquad (2)$$

Equation (1) is developed from the assumption that the porous media is made of mono-dispersed sphere particles. The permeability, k, is made dimensionless by using the cylinder diameter D to be expressed by the Darcy number, $Da = k/D^2$. The permeability is related to the porosity, and the particle diameter, d_p, through

$$k = \frac{^3 d_p}{a(1 \quad)^2} \ . \qquad (3)$$

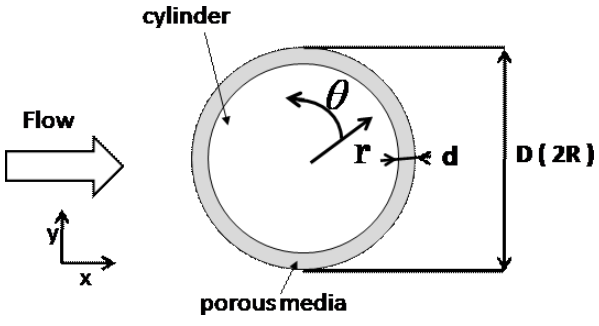

Figure 1: Flow configuration.

Note that, since Eq. (1) reduces to the conventional Navier-Stokes equation outside the porous media, the interface between the porous media and flow outside can be solved without any additional treatment. Throughout the present study, the surrounding porous media are assumed to have uniform thickness, permeability, and porosity. Two different thicknesses are considered: 20% and 50% of whole radius (i.e., $d = 0.2R$ and $d = 0.5R$).

The simulation code is based on the DNS code in the cylindrical coordinate system by Fukagata and Kasagi (2002). The governing equation is spatially discretized by the finite difference method: the energy conservative second-order central difference scheme and the second order central difference scheme are applied for the convection and diffusion terms, respectively. The low-storage third order Runge-Kutta/Crank-Nicolson (RK3/CN) scheme is used for the time integration. The velocity and the pressure are coupled by the delta form fractional step method. The pressure Poisson equation is solved by using the Fast Fourier Transform(FFT) in the azimuthal ( ) and axial (z) directions and the tridiagonal matrix algorithm (TDMA) in the radial (r) direction. A uniform velocity, U , is imposed at the inlet boundary ($\frac{1}{4}\pi \leq \leq \frac{3}{4}\pi$), and the convective velocity condition is used at the outlet boundary ($\frac{3}{4}\pi \leq \leq \frac{1}{4}\pi$). Information on the number of cells and the computational domain used is shown in Table 1.

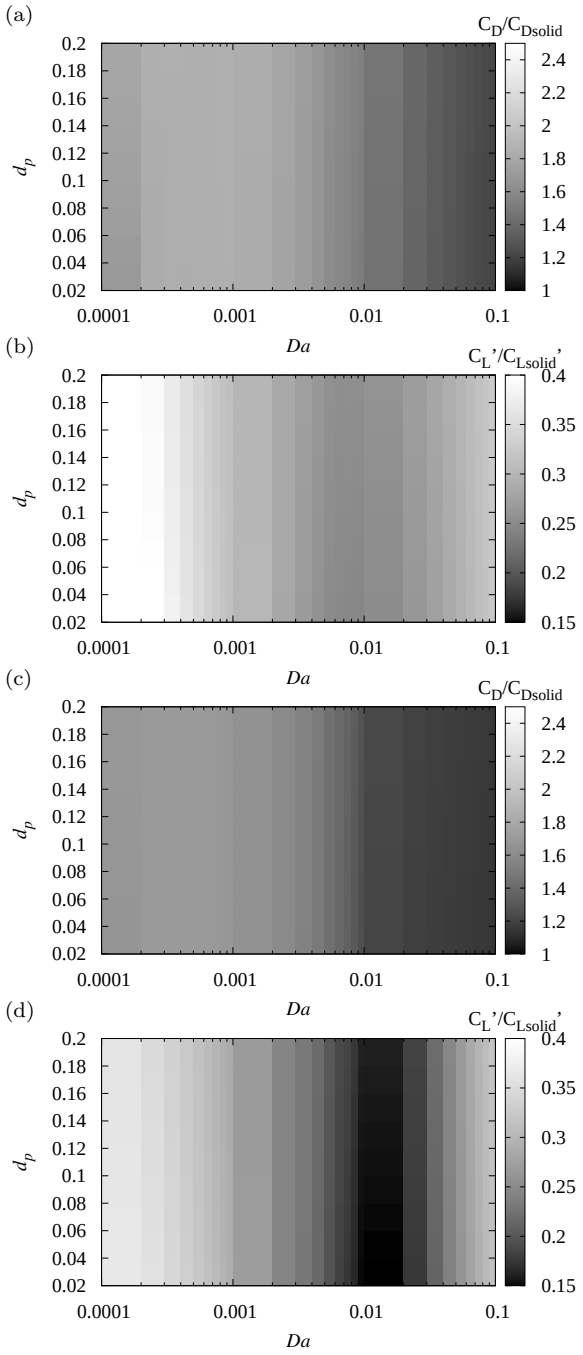

Figure 2: Normalized drag and rms lift coefficients, C_D and C_L', computed under different values of Darcy number, Da, and dimensionless particle diameter, d_p (2D simulation, $Re = 1000$): (a) C_D for porous media thickness of $d = 0.2R$; (b) C_L' for $d = 0.2R$; (c) C_D for $d = 0.5R$; (d) C_L' for $d = 0.5R$.

Table 1: Information of computational domain

	$N_r \times N \times N_z$	$L_r \times L_z$
DNS (Solid)	$270 \times 256 \times 64$	$70D \times \pi D$
DNS (Porous $d = 0.2R$)	$310 \times 256 \times 64$	$70D \times \pi D$
DNS (Porous $d = 0.5R$)	$370 \times 256 \times 64$	$70D \times \pi D$
LES (Porous $d = 0.5R$)	$200 \times 256 \times 16$	$30D \times \pi D/4$

RESULTS AND DISCUSSION

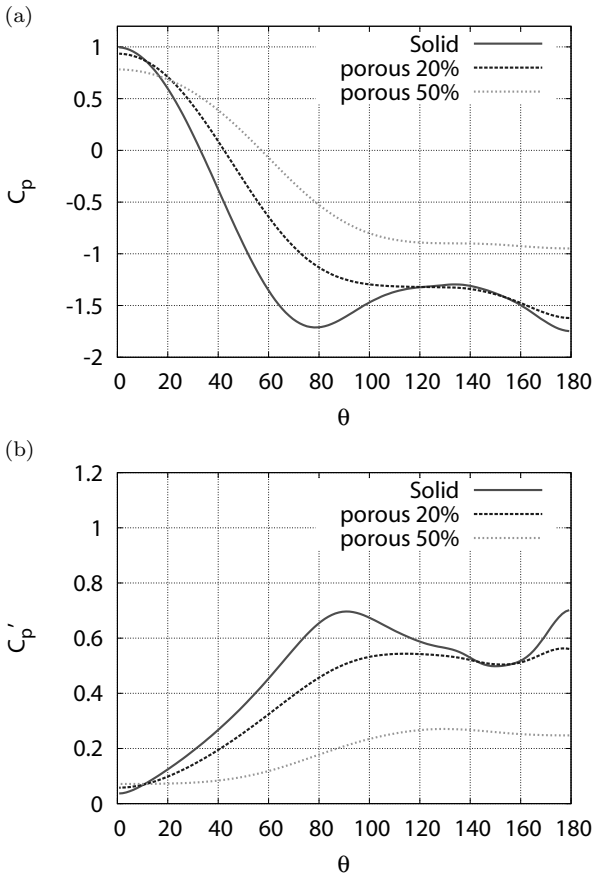

Figure 3: Pressure distribution on the surface (2D simulation, $Re = 1000$): (a) time averaged pressure, C_p; (b) rms pressure fluctuations, C_p'.

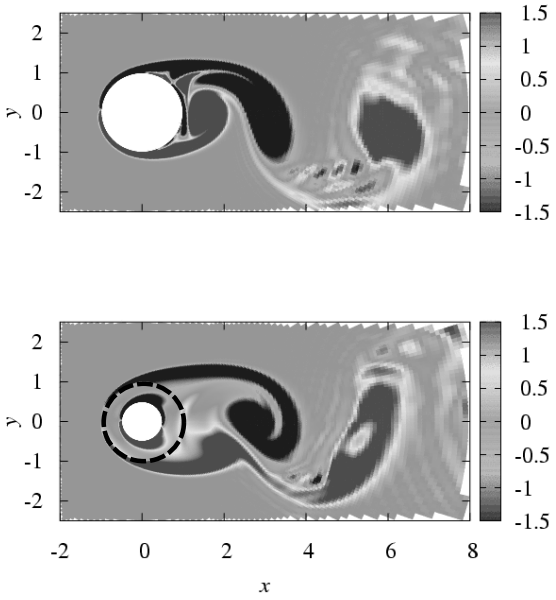

Figure 4: Distribution of vorticity, (2D simulation, $Re = 1000$): (a) solid; (b) $d = 0.5R$ (dashed line denotes the surface of porous media).

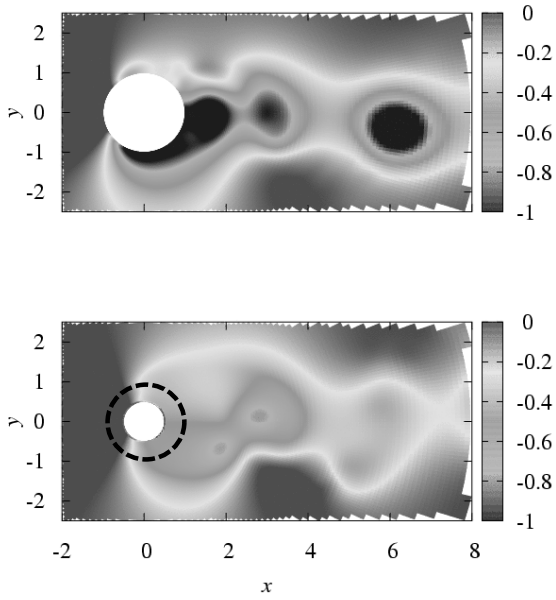

Figure 5: Pressure distribution, C_p (2D simulation, $Re = 1000$): (a) solid; (b) $d = 0.5R$ (dashed line denote surface of porous media).

Parametric test

First of all, a parametric test is performed by 2D DNS in order to find the most effective properties of surrounding porous media, In particular, we focus on the effect of dimensionless permeability, Da, and the particle diameter, d_p. The Reynolds number based on the freestream velocity and the outer diamter of the cylinder including the porous part is set at $Re = 1000$, in which vortex-shedding clearly occurs. In total, 280 cases are simulated with 28 different values of Da in the range of $1.0\times10^{-4} \le Da \le 1.0\times10^{-1}$ and 10 different values of d_p in the range of $2.0 \times 10^{-2} \le d_p \le 2.0 \times 10^{-1}$.

The effect of Da and d_p are evaluated by the time-averaged drag coefficient, C_D, and the root-mean-square (rms) of lift force coefficient, C'_L, defined respectively as

$$C_D = \frac{\overline{F_x}}{\frac{1}{2}\rho U^2} , \qquad C'_L = \frac{\sqrt{\overline{(F'_y)^2}}}{\frac{1}{2}\rho U^2} , \tag{4}$$

where F_x and F_y denote the force components in the streamwise and the perpendicular directions, respectively; the overbar and the prime denote the temporal mean and the fluctuation, respectively. The force subjected to cylinder surrounded by porous media, F, is calculated by the following equation obtained by integrating Eq. (1):

$$F = \oint_\Omega pnds + \oint_\Omega ds + \int_\Omega K dv , \tag{5}$$

where n is the unit vector normal to the porous surface, $\partial\Omega$.

Figure 2 shows the results of parametric test. The drag and rms lift coefficients, C_D and C'_L, are normalized by the values of the solid case, $C_{D\ solid}$ and $C'_{L\ solid}$. These figures show that both C_D and C'_L are more sensitive to Da than d_p. In the case of $d = 0.2R$, C_D is found to be always greater than that of the solid case, while $C'_L/C'_{L\ solid}$ becomes smaller than unity. For $d = 0.5R$, the effect of C'_L is more noticeable. Especially, in the case of $Da = 1.0 \times 10^{-2}$, $d_p = 2.0 \times 10^{-2}$, and $= 0.99$, C'_L is reduced to 14% of $C'_{L\ solid}$.

Profiles of 2D flow ($Re = 1000$)

In order to investigate detailed effects of porous surface to the flow, we focus on the case where the largest reduction of C'_L was obtained, i.e., $Da = 1.0 \times 10^{-2}$, $d_p = 2.0 \times 10^{-2}$, and $= 0.99$.

Figure 3(a) shows the time averaged pressure distribution on the cylinder surface. As is well known, the pressure distribution of the solid case has a local minimum around 80 . On the other hand, with the porous surface (regardless of its thickness, i.e., $d = 0.2R$ and $d = 0.5R$), such a local minimum point is not observed. The pressure distribution in the front side are increased and this causes the drag increase as observed in Fig. 2.

Figure 3(b) shows the pressure fluctuation on the surface, C'_p. It is apparent that the pressure fluctuation is suppressed by the porous media. Application of the thicker porous surface ($d = 0.5R$) seems to be more effective than the thinner ($d = 0.2R$). The reduction of C'_L observed in Fig. 2 is attibuted to this reduction of pressure fluctuation.

Figure 4 shows the vorticity fields at the time instants when the lift forces take the maximum values. Although separation on the surface and accompanied vortex shedding are observed in both cases, the vortices are more detached in the porous case.

The difference is clearer for the pressure distribution, as shown in Fig. 5. The low pressure region, which extends over cylinder surface in the solid case, is significantly weakened in the porous case. The porous surface is found to stabilize the flow oscillation around the cylinder and weaken the vortices shed therefrom.

Flow modification can also be seen in the velocity profile of downstream wake. Development of the mean streamwise velocities are compared in Fig. 6(a). In the solid case, the streamwise velocity, $< u >$, decelerates near the cylinder and it gradually recoveres in the downstream region. In the cases of porous surface, the velocity profile shows peculiar behavior. The velocity deficit recovers once around $x/D = 3$ similarly to the solid case. In the further downstream region,

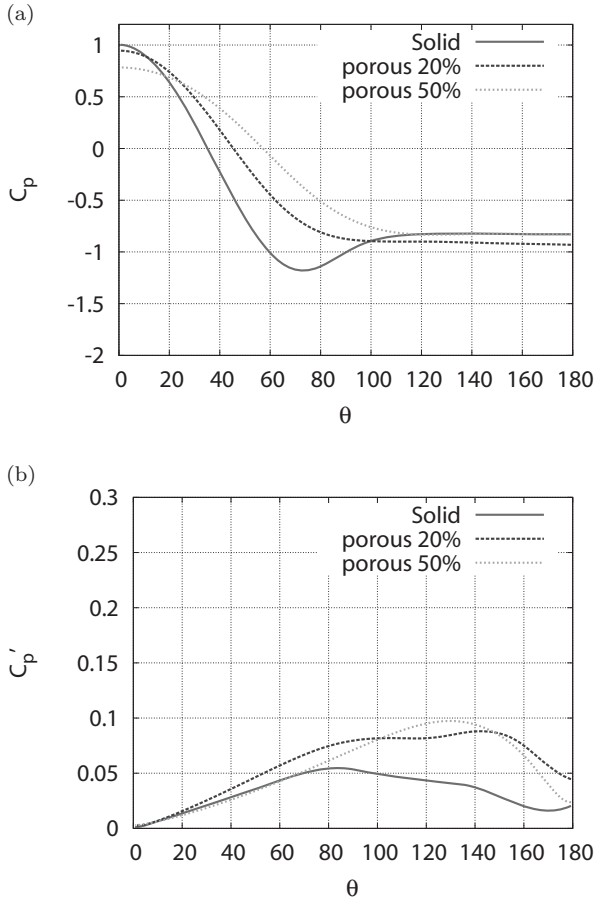

Figure 7: Pressure distribution on the surface (3D DNS, $Re = 1000$): (a) time averaged pressure, C_p; (b) rms of pressure fluctuations, C_p'

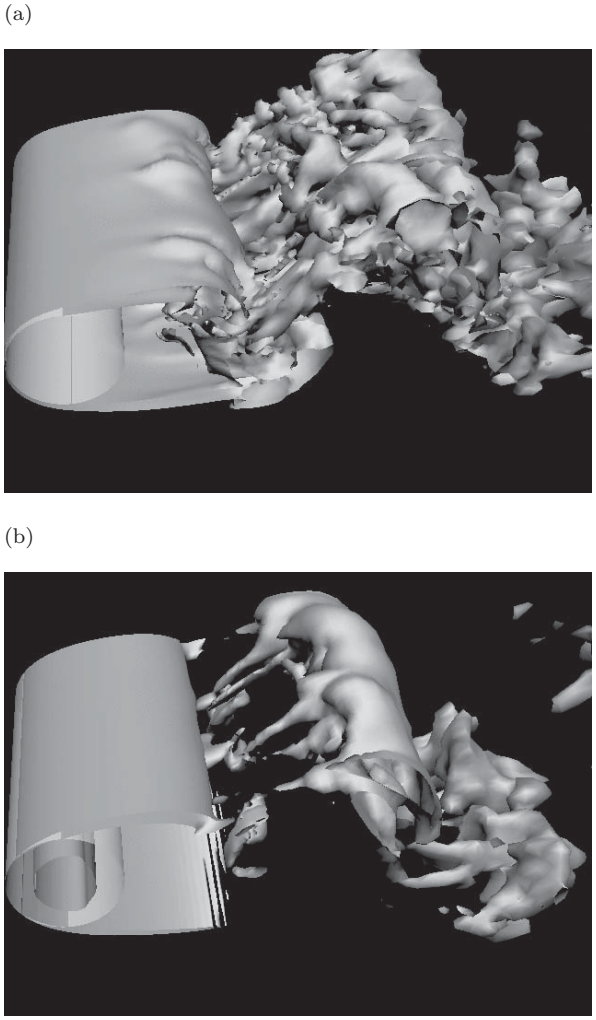

Figure 8: Isosurface of vorticity, ω (3D DNS, $Re = 1000$): (a) solid; (b) $d = 0.5R$.

say $x/D = 6$, however, the velocity deficit develops again. As shown in Fig. 6(b), the perpendicular velocity, $< v >$, is accelerated in the far wake region: $< v >$ is positive for $y > 0$ and negative for $y < 0$, which makes the streams directed away from the centerline.

Profiles of 3D flow ($Re = 1000$)

Generally speaking, the flow in the wake of the cylinder involves intensive three dimensionality at $Re \gtrsim 190$ (Williamson, 1996), and such 3D effects are expected to propagate back to the cylinder surface upstream. Here, we present the results obtained by 3D DNS at $Re = 1000$ and compare them with the 2D results presented above.

Figure 7(a) shows the distributions of mean surface pressure. Smoothing of the distribution observed in the 2D flow is also observed in the 3D flow. Base pressure of the solid case and $d = 0.2R$ case is found to be remarkably increased in 3D flow as compared to the 2D case, whereas the base pressure is less increased in $d = 0.5$ case,

The rms pressure fluctuation is shown in Fig. 7(b). The profile is modified the similar manner as in the 2D flow, but the amount of modification is smaller due to the 3D development of the wake.

The 3D characteristics of the wake of clearly illustrated by the isosurface of vorticity, as shown in Fig. 8. With the porous surface, disturbances in the wake are remarkably suppressed. While the shear layer in the solid case has strong 3D structure, such as streamwise vortices, such 3D behavior is suppressed in the case of $d = 0.5R$. For an ordinary (i.e., solid) cylinder, the flow stays 2D at lower Reynolds number and goes through transition to 3D at a critical Reynolds number, which is far below the Reynolds number considered here. The present result shows that flow around a cylinder with porous media is stabilized as if the Reynolds number were reduced.

Reynolds number dependency

Simulation is performed at different Reynolds numbers, i.e., 100 and 1.0×10^5, in order to investigate the dependency on the Reynolds number. The property of porous media unchanged from the simulation at $Re = 1000$ presented above, i.e., $Da = 1.0 \times 10^{-2}$, $d_p = 2.0 \times 10^{-2}$, and $\phi = 0.99$.

Low Reynolds number flow ($Re = 100$). Figure 9 shows the distributions of mean and rms pressure coefficients on the surface. As can be judged from the location of minimum value of mean pressure coefficient, the separation is hindered by applying the porous media. The drastic change of profile observed at $Re = 1000$, however, is not observed either in

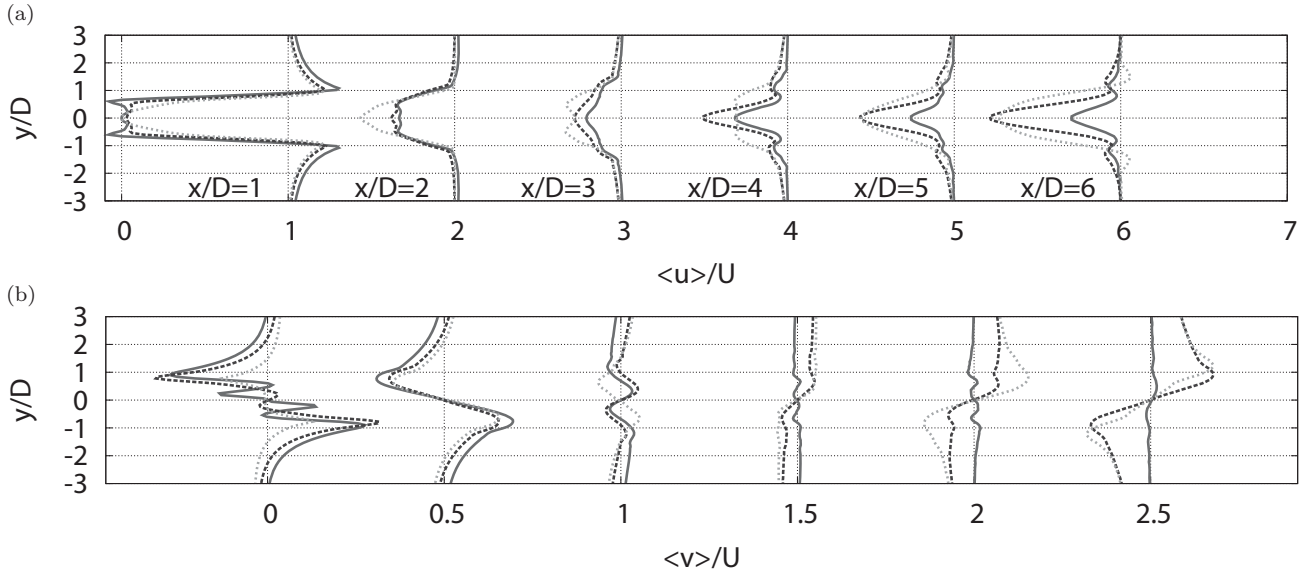

Figure 6: Mean velocity profiles (2D simulation, $Re = 1000$): (a) streamwise component; (b) perpendicular component. Solid line, solid case; black dotted line, $d = 0.2R$; gray dotted line, $d = 0.5R$.

the mean or the rms profile.

The velocity profiles in the downstream region are shown in Fig. 10. Slight difference can be observed between the solid and porous cases in the vicinity of the cylinder. The difference, however, becomes smaller in the downstream region and no clear difference is observed between them at $x/D = 6$.

High Reynolds number flow ($Re = 1.0 \times 10^5$). The effect of porous media at $Re = 1.0 \times 10^5$, which is the same as the previous experiment of Takaishi et al. (2007), is studied by means of large-eddy simulation.

The constant Smagorinsky model with the Smagorinsky constant of $C = 0.1$ is used together with the van Driest damping function in the region near the cylinder wall.

Contour of the instantaneous vorticity field is shown in Fig. 11. It is observed that the two thin shear layer separating on the surface grows parallely toward downstream. These shear layers never rolls up, which means that the vortex shedding is completely suppressed. And this stabilized flow pattern looks quite similar to the result of PIV measurement by Takaishi et al. (2007), although detailed comparison should made in the future.

SUMMARY AND MECHANISM OF FLOW STABILIZATION

We carried out numerical simulation of flow around a circular cylinder surrounded by porous media.

The most effective parameters of porous media was found by two-dimensional (2D) parametric test at $Re = 1000$. Notable suppression of the lift force fluctuation is obtained in the case of thicker porous surface. The flow statistics show that the mean and the fluctuate pressure distributions on the wall are significantly modified. The stabilized shear layer similar to that in the 2D is also observed in the three-dimensional (3D) simulation at the same Reynolds number, i.e., $Re = 1000$, although the effect of porous media is weakened due to the inherent 3D characteristics of the wake flow development. The comparison among the results at different Reynolds numbers reveals that the stabilizing effect of porous surface works better at higher Reynolds numbers.

To conclude this paper, we refer to a possible mechanism of flow stabilization. The flow around a circular cylinder shedding vortex exhibits periodic change, which accompanies a periodic change of stress to the control volume adjacent to the surface. Thus, the flow system is roughly modeled as a self-oscillatory system with a mass and a spring.

Introduction of the porous media to system is similar to add a damper, as shown in Fig. 12, which works proportional to the velocity following to Darcy's law, i.e.,

$$\Delta p = -\frac{\mu}{k} U_{bulk} \ , \tag{6}$$

which stabilizes the system. This direct mechanism should be realized only in the proximity of the porous surface. This mechanism is conjectured to work well when the boundary layer is thinner and vorticity is concentrated in the proximity of the surface. On the other hand, it may not work when the boundary layer is much thicker than the thickness where the damper has its direct influence. This mechanism may explain the Reynolds number dependency observed in the present study.

ACKNOWLEGMENT

KF wishes to thank Dr. Takehisa Takaishi (Railway Technical Research Institute, Japan) for fruitful discussions, which motivated the present study.

REFERENCES

Brewer, M., 2000, "A challenging test case for large eddy simulaation: high Reynolds number circular cylinder flow", *Int. J. Heat Fluid Flow*, Vol. 21, pp. 648-654.

Bruneau, C-H. and Mortazavi, i., 2004, "Passive control of flow around a square cylinder using porous media" *Int. J. Numer. Meth. Fluids*, Vol. 46, pp. 415-433.

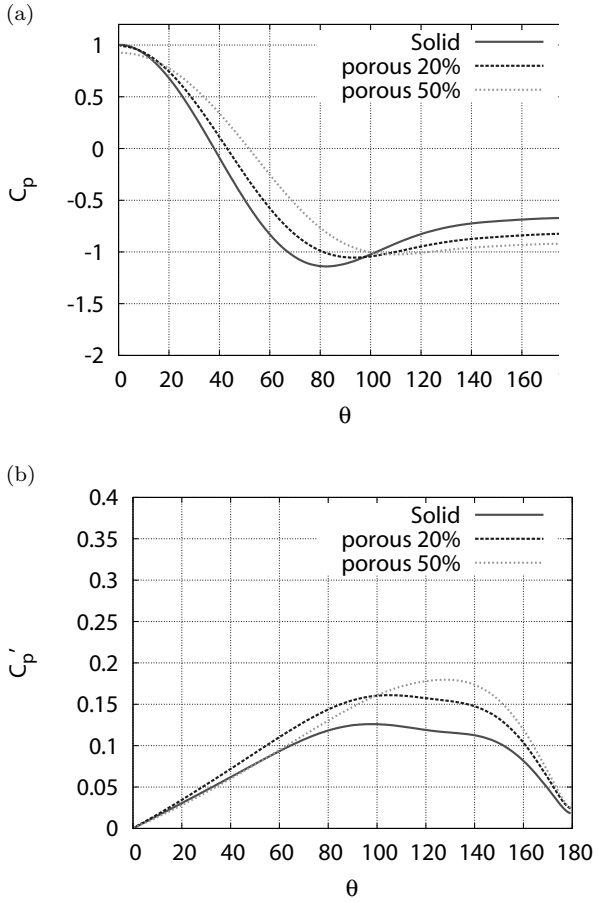

Figure 9: Pressure distribution on the surface ($Re = 100$): (a) time averaged pressure, C_p; (b) rms of pressure fluctuations, C_p'.

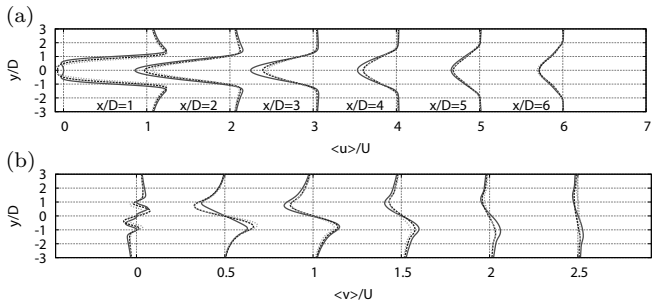

Figure 10: Mean velocity profiles (3D DNS, $Re = 100$).

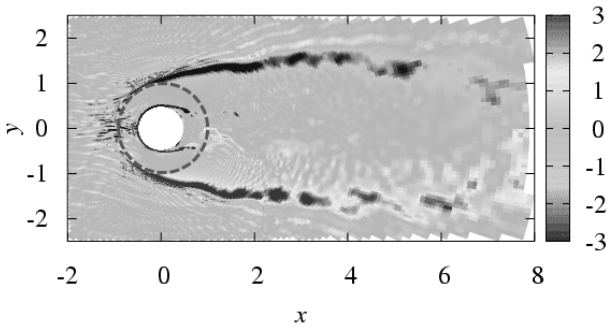

Figure 11: Distribution of vorticity, (3D LES. $Re = 10^5$): (a) solid ;(b) $d = 0.5R$(dashed line denote surface of porous media).

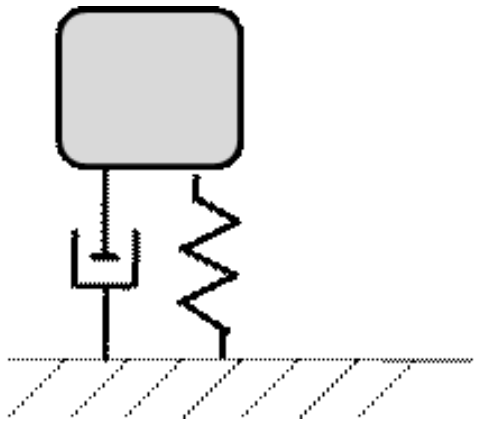

Figure 12: Mechanism of flow stabilization.

Choi, H., Jeon, W.-P., and Kim. J., 2008, "Control of flow over a bluff body", *Annu. Rev. Fluid Mech.*, Vol. 40, pp. 113-139.

Fukagata, K. and Kasagi, N., 2002, "Highly energy-conservative finite difference method for the cylindrical coordinate system", *J. Comput. Phys.*, Vol. 181, pp. 478-498.

Hsu, C. T. and Cheng, P., 1990, "Thermal dispersion in porous medium", *Int. J. Heat Mass Transfer*, Vol. 33, pp. 1587-1597.

Jiménez, J., Uhlmann, M. Pinelli, A. and Kawamura, G., 2001, "Turbulent shear flow over active and passive porous surfaces" *J. Fluid Mech.*, Vol. 442 pp. 89-117.

Martys, S. N. and Chen, H., 1996 "Simulation of multicomponent fluids in complex three-dimensional geometries by the lattice Boltzmann method", *Phys. Rev. E*, Vol. 53, pp. 743-752.

Sueki,K., Takaishi, T. and Ikeda, M., 2007, "Technique of aerodynamic noise reduction by porous material (1st report: Experimental results of aerodynamic sound and aerodynamic force)" Proc. JSME-FED Annu. Conf. 2007, Paper No. 103, 4 pp. (in Japanese)

Takaishi, T., Sueki,K. and Ikeda, M., 2007, "Technique of aerodynamic noise reduction by porous material (2nd report: Experimenatal results of wake velocities and characteristics of sound absorption)", 2007, Proc. JSME-FED Annu. Conf. 2007, Paper No.104, 4 pp. (in Japanese)

Williamson, C. H. K., 1996, "Vortex dynamics in the cylinder wake" *Annu. Rev. Fluid. Mech.*, Vol. 28, pp. 477-539.